Estimating total magnetization direction using equivalent-layer technique

André L. A. Reis[†] [*], **Vanderlei C. Oliveira Jr.**[†] **and Valéria C. F. Barbosa** [†]

[†] *Observatório Nacional, Rio de Janeiro, Brazil*

[*] *Corresponding author: reisandreluis@gmail.com*

(August 9, 2019)

GEO-2019XXXX

Running head: **Determining total magnetization direction**

ABSTRACT

We developed a new method for estimating the total magnetization direction of magnetic sources based on equivalent layer technique using total-field anomaly data. In this approach, we do not have to impose strong information about the shape and the depth of the sources neither require a regularly spaced data. Usually, this technique is used for processing potential data estimating a 2D magnetic-moment distribution over a fictitious layer composed by dipoles below the observation plane. In certain conditions, when the magnetization direction of equivalent sources is almost the same as the true body, the estimated magnetic property over the layer is all positive. Our method uses this remarkable feature to estimate a nonnegative magnetic-moment distribution over the layer and a magnetization direction through an iterative process. Therefore, we propose a nested algorithm to solve the inverse problem in two steps. We test the methodology by applying to synthetic data for complicated geological scenarios. Moreover, we applied the method to field data from Goias Alkaline Province (GAP), center of Brazil, over Montes Claros complex.

METHODOLOGY

Fundamentals of magnetic equivalent layer and the positive magnetic-moment distribution

Considering a Cartesian coordinate system with x-, y- and z-axis being oriented to north, east and downward, respectively. Let $\Delta T_i \equiv \Delta T(x_i, y_i, z_i)$ be the total-field anomaly, at the ith position (x_i, y_i, z_i), produced by a continuos layer located below the observation plane at a depth equal to z_c, where $z_c > z_i$, and $p(x', y', z_c)$ is the distribution of magnetic dipoles moment per unit area over the layer. The total-field anomaly produced by this continuous layer is given by

$$\Delta T_i = \int_{-\infty}^{+\infty}\int_{-\infty}^{+\infty} p(x', y', z_c)[\gamma_m \hat{\mathbf{F}}_0^T \mathbf{M}(x_i, y_i, z_i, x', y', z_c)\, \hat{\mathbf{m}}(\mathbf{q})]dx'\, dy', \tag{1}$$

where γ_m is a constant proportional to the vacuum permeability, $\hat{\mathbf{F}}_0$ is a unit vector with the same direction of the main geomagnetic field given by

$$\hat{\mathbf{F}}_0 = \begin{bmatrix} \cos I \cos D \\ \cos I \sin D \\ \sin I \end{bmatrix}, \tag{2}$$

where I and D are, respectively, the inclination and declination and $\mathbf{M}(x_i, y_i, z_i, x', y', z_c)$ is a 3×3 dimensional matrix (Oliveira Jr et al., 2015) equal to

$$\mathbf{M}(x_i, y_i, z_i, x', y', z_c) = \begin{bmatrix} \partial_{xx}\phi & \partial_{xy}\phi & \partial_{xz}\phi \\ \partial_{yx}\phi & \partial_{yy}\phi & \partial_{yz}\phi \\ \partial_{zx}\phi & \partial_{zy}\phi & \partial_{zz}\phi \end{bmatrix}, \tag{3}$$

where $\partial_{\alpha\beta}\phi$, $\alpha = x, y, z$ and $\beta = x, y, z$, is the second derivative of the scalar function

$$\phi(x_i, y_i, z_i, x', y', z_c) = \frac{1}{[(x_i - x')^2 + (y_i - y')^2 + (z_i - z_c)^2]^{\frac{1}{2}}}. \tag{4}$$

with respect to the Cartesian coordinates x_i, y_i and z_i of the observation points. The $\hat{\mathbf{m}}(\mathbf{q})$ is a unit vector with the magnetization direction of the dipoles over layer given by

$$\hat{\mathbf{m}}(\mathbf{q}) = \begin{bmatrix} \cos\tilde{\imath}\cos\tilde{d} \\ \cos\tilde{\imath}\sin\tilde{d} \\ \sin\tilde{\imath} \end{bmatrix} \tag{5}$$

and $\mathbf{q}$ is a 2×1 vector with components given by

$$\mathbf{q} = \begin{bmatrix} \tilde{\imath} \\ \tilde{d} \end{bmatrix}, \tag{6}$$

where $\tilde{\imath}$ and $\tilde{d}$ are the inclination and declination of the magnetization direction of the dipoles on the layer, respectively. We can also notice that the vector defined in equation 5 has a single and uniform magnetization direction of all dipoles on the layer. For convenience, this unit vector can be rewritten as follows

$$\hat{\mathbf{m}}(\mathbf{q}) = \mathbf{R}\hat{\mathbf{h}}\,, \tag{7}$$

where $\hat{\mathbf{h}}$ defines the uniform magnetization direction of an abitrary magnetic source and $\mathbf{R}$ is a 3×3 matrix obtained from Euler's rotation theorem. This theorem states that any rotation can be parametrized by using three parameters called Euler angles (H. Goldstein and Safko, 1980). That is, if all dipoles that set up the equivalent layer have the same magnetization direction $\hat{\mathbf{m}}(\mathbf{q})$ and this direction is the same as the true magnetic source $\hat{\mathbf{h}}$,

then the matrix $\mathbf{R}$ (equation 7) is equal to identity. For this reason, the total-field anomaly produced by equivalent layer at the ith position (x_i, y_i, z_i) (equation 1) can be rewritten as

$$\Delta T_i = \int_{-\infty}^{+\infty}\int_{-\infty}^{+\infty} p(x', y', z_c)[\gamma_m \hat{\mathbf{F}}_0^T \mathbf{M}(x_i, y_i, z_i, x', y', z_c)\,\hat{\mathbf{h}}]dx'\,dy', \tag{8}$$

which represents the total-field anomaly produced by continuous layer with the same direction of the arbitrary magnetic source. Thus, the RTP field ΔT_i^{PL} produced by equivalent layer at the point (x_i, y_i, z_i) is equal to

$$\Delta T_i^{PL} = \int_{-\infty}^{+\infty}\int_{-\infty}^{+\infty} p(x', y', z_c)[\gamma_m \partial_{zz}\phi(x_i, y_i, z_i, x', y', z_c)]dx'\,dy', \tag{9}$$

where $\partial_{zz}\phi(x_i, y_i, z_i, x', y', z_c)$ is the second derivative of the inverse of distance (equation 4) with respect of z_i, evaluated at the point (x_i, y_i, z_i). However, by considering the RTP field ΔT_i^{PS} that would be produced by an arbitrary uniformly magnetized source at the pole, we have

$$\Delta T_i^{PS} = \gamma_m \partial_{zz}\Gamma(x_i, y_i, z_i)\, m, \tag{10}$$

where m is the magnetization intensity of the magnetic source. The $\partial_{zz}\Gamma(x_i, y_i, z_i)$ is the second derivative in relation to z_i of a scalar function $\Gamma(x_i, y_i, z_i)$

$$\Gamma(x_i, y_i, z_i) = \iiint_{\upsilon} \frac{d\upsilon}{[(x_i-\alpha)^2 + (y_i-\beta)^2 + (z_i-\gamma)^2]^{\frac{1}{2}}} \tag{11}$$

in which α, β and γ are the Cartesian coordinates of an infinitesimal element inside the volume υ of the magnetic source. From equation 9 and 10, we obtain

$$m\,\partial_{zz}\Gamma(x_i, y_i, z_i) = \int_{-\infty}^{+\infty}\int_{-\infty}^{+\infty} p(x', y', z_c)\partial_{zz}\phi(x_i, y_i, z_i, x', y', z_c)dx'\,dy'. \tag{12}$$

We can notice that equation 12 can be calculated differentiating the following equation

$$m\,\partial_{z}\Gamma(x_i, y_i, z_i) = \int_{-\infty}^{+\infty}\int_{-\infty}^{+\infty} \frac{p(x', y', z_c)(z_c - z_i)}{[(x_i - x')^2 + (y_i - y')^2 + (z_i - z_c)^2]^{\frac{3}{2}}}dx'\,dy', \tag{13}$$

where $z_c > z_i$, with respect to the vertical component z_i.

From potential-field theory, we can highlight the classical upward continuation integral

$$U(x_i, y_i, z_i) = \frac{(z_c - z_i)}{2\pi}\int_{-\infty}^{+\infty}\int_{-\infty}^{+\infty} \frac{U(x', y', z_c)}{[(x_i - x')^2 + (y_i - y')^2 + (z_i - z_c)^2]^{\frac{3}{2}}}dx'\,dy', \tag{14}$$

where the function $U(x_i, y_i, z_i)$ is an hamornic function at all (x_i, y_i, z_i) and $U(x', y', z_c)$ is the same harmonic function ate (x', y', z_c) (Blakely, 1996). In this case, if this harmonic function represents the total-field anomaly at the point (x_i, y_i, z_i), it can be mathematically interpreted as the convolution between its values $U(x', y', z_c)$ and the vertical derivative in relation to z_i of the equation 4, evaluated on the horizontal plane $z_i = z_c$. Therefore, according to the classical upward continuation function (equation 14), the magnetic-moment distribution $p(x', y', z_c)$ in equation 13 assumes the form

$$p(x', y', z_c) = \frac{m}{2\pi}\,\partial_z\Gamma(x', y', z_c), \tag{15}$$

where $\partial_z\Gamma(x', y', z_c)$ is the derivative of the scalar function 11 in relation to z_i evaluated over the equivalent layer. The most interesting aspect of equation 15 is that the magnetic-moment distribution is defined as the product of a positive constant $\frac{m}{2\pi}$ and the function $\partial_z\Gamma(x', y', z_c)$, which is all positive at all points (x', y', z_c) over the equivalent layer.

This relation is similar to that presented by Pedersen (1991) and Li et al. (2014). In the wavenumber domain, these authors determined the magnetic-moment distribution within a continuous equivalent layer with the same magnetization direction as the local-geomagnetic field at the pole. They also considered a planar equivalent layer located below and parallel to a horizontal plane containing the observed total-field anomaly. They assume a magnetic source having a purely induced magnetization. Under these assumptions, Pedersen (1991) and Li et al. (2014) concluded that the magnetic-moment distribution within the continuous equivalent layer is proportional to the pseudogravity anomaly produced by the source on the plane of the equivalent layer. By following different approaches using magnetic microscopy data, Baratchart et al. (2013) and Lima and Weiss (2016) pointed out by imposing a non-negativity constraint, the solution to the inverse problem is a unique magnetic-moment distribution. Here we do not follow the same wavenumber-domain reasoning used by all these authors. Moreover, equation 15 generalizes this positivity condition because (1) it holds true for all cases in which the magnetization of the equivalent layer has the same direction as the true magnetization of the sources, regardless it is purely induced or not, (2) does not require that the observed total-field anomaly data be on a plane and, (3) does not require a planar equivalent layer.

Parametrization and forward problem

In practical situations, its not possible to determine a continuous magnetic-moment distribution $p(x', y', z_c)$ over the layer as shown in equation 1. For this reason, the layer has to be approximated by a discrete set of dipoles with unit volume located at a constant depth $z = z_c$. By discretizing the integrand of equation 1, the predicted total-field anomaly at the point (x_i, y_i, z_i) is given by

$$\Delta T_i = f_i(\mathbf{s}), \tag{16}$$

where ΔT_i is the ith element of the N-dimensional vector of predicted total-field anomaly $\mathbf{\Delta T}(\mathbf{s})$. The function f_i maps the unknown parameters onto the data, in which the parameter vector $\mathbf{s}$ is formed by an M-dimensional vector $\mathbf{p}$ whose jth element p_j is the magnetic moment of the jth dipole with a single magnetization direction $\mathbf{q}$ (equation 6) assigned to all dipoles (figure 1). Explicitly, the function f_i is described as

$$f_i(\mathbf{s}) = \sum_{j=1}^{M} p_j g_{ij}(\mathbf{q}) = \mathbf{p}^T \mathbf{g}_i(\mathbf{q}), \tag{17}$$

where

$$g_{ij}(\mathbf{q}) = \gamma_m \hat{\mathbf{F}}_0^T \mathbf{M}_{ij} \hat{\mathbf{m}}(\mathbf{q}) \tag{18}$$

is an harmonic function representing the total-field anomaly at the ith position (x_i, y_i, z_i) yielded by a jth dipole located at (x_j, y_j, z_c) with unit magnetic-moment intensity. The matrix $\mathbf{M}_{ij}$ is formed by the second derivatives of a function ϕ_{ij} that depends on the inverse of the scalar function $r_{ij} = [(x_i - x_j)^2 + (y_i - y_j)^2 + (z_i - z_c)^2]^{1/2}$, analogously to equations 3 and 4. From equations 16-18, we can notice that the predicted total-field anomaly $\mathbf{\Delta T}(\mathbf{s})$ has a linear relation with the magnetic moment $\mathbf{p}$ and a nonlinear relation with the magnetizaion direction $\mathbf{q}$.

Inverse problem

Let $\mathbf{\Delta T}^o$ be an N-dimensional vector whose ith element ΔT_i^o is the total-field anomaly observation produced by a magnetic source at the point (x_i, y_i, z_i), $i = 1, \ldots, N$. In order to

estimate the magnetization direction, we have to formulate an inverse problem by imposing a positivity constraint on the magnetic-moment distribution. It can be performed minimizing the difference between the observed data $\mathbf{\Delta T}^o$ and the predicted data $\mathbf{\Delta T}(\mathbf{s})$ by solving the following constrained problem of

$$\text{minimizing} \qquad \Psi(\mathbf{s}) = \|\mathbf{\Delta T}^o - \mathbf{\Delta T}(\mathbf{s})\|_2^2 + \mu f_0 \parallel \mathbf{p} \parallel_2^2 \tag{19a}$$

$$\text{subject to} \qquad \mathbf{p} \geqslant 0. \tag{19b}$$

On the right side of equation 19a the first and second terms are the data-misfit function and the zeroth-order Tikhonov regularization function, μ is the regularizing parameter, $\|\cdot\|_2^2$ represents the squared Euclidean norm and f_0 is a normalizing factor. In the inequality 19b, $\mathbf{0}$ is a null vector and the inequality sign is applied element by element. This inequality imposes positivity constraints on the estimated magnetic moments of all dipoles, which is solved by using the nonnegative least squares (NNLS) proposed by Lawson and Hanson (1974).

Minimizing the goal function shown in equation 19a starts with an initial approximation $\mathbf{s}^k$ to the parameter vector and then solving a sequence of linear problem of estimating a correction $\mathbf{\Delta s}^k$ at each kth iteration. The procedure is repeated until a minimum of goal function (equation 19a) is reached. This procedure is determined by using a gradient-based iterative optimization method like Gauss-Newton (Aster et al., 2005). Mathematically, the correction $\mathbf{\Delta s}^k$ is expressed as a second-order expansion of the goal function given by

$$\Psi(\mathbf{s}^k + \mathbf{\Delta s}^k) \approx \Psi(\mathbf{s}^k) + \mathbf{J}^{k^T}(\mathbf{s}^k)\mathbf{\Delta s}^k + \frac{1}{2}\mathbf{\Delta s}^{k^T}\mathbf{H}^k(\mathbf{s}^k)\mathbf{\Delta s}^k \tag{20}$$

in which $\mathbf{J}^k(\mathbf{s}^k)$ and $\mathbf{H}^k(\mathbf{s}^k)$ are, respectively, the gradient vector and the Hessian matrix

of equation 19a. Thus, taking the gradient of the function 20, the parameter perturbation vector $\mathbf{\Delta s}^k$ at the kth iteration is obtained by solving the linear system

$$\mathbf{H}^k(\mathbf{s}^k)\mathbf{\Delta s}^k = -\mathbf{J}^k(\mathbf{s}^k), \tag{21}$$

where the estimate $\mathbf{\Delta s}^k$ is a single step of the Gauss-Newton method required to attain the minimum of the expanded function (equation 20). The linear system given by equation 21 can be rewritten as

$$\left[\begin{array}{c|c} \mathbf{H}^k_{pp} & \mathbf{H}^k_{pq} \\ \hline \mathbf{H}^k_{qp} & \mathbf{H}^k_{qq} \end{array}\right] \left[\begin{array}{c} \mathbf{\Delta p}^k \\ \\ \mathbf{\Delta q}^k \end{array}\right] = - \left[\begin{array}{c} \mathbf{J}^k_p \\ \\ \mathbf{J}^k_q \end{array}\right], \tag{22}$$

in which $\mathbf{J}^k_\alpha$ and $\mathbf{H}^k_{\alpha\beta}$, where $\alpha = p, q$ and $\beta = p, q$, are the gradient vector and the Hessian matrix calculated in relation to each component of the magnetic-moment vector $\mathbf{p}$ and the magnetization direction vector $\mathbf{q}$, respectively. Besides, in order to simplify the linear system 22, we consider null cross-derivatives.

However, the gradient vector and the Hessian matrix relative to the part of magnetic moments are, respectively,

$$\mathbf{J}^k_p = -2\mathbf{G}^{k^T}_p [\mathbf{\Delta T}^o - \mathbf{\Delta T}(\mathbf{s}^k)] + 2\mu f^k_0 \mathbf{p}^k \tag{23}$$

and

$$\mathbf{H}^k_{pp} = 2\mathbf{G}^{k^T}_p \mathbf{G}^k_p + 2\mu f^k_0 \mathbf{I} \tag{24}$$

where $\mathbf{G}^k_p$ is the $N \times M$ sensitivity matrix at the kth iteration, whose elements are composed by the derivative of equation 19a in relation of jth element of the vector $\mathbf{p}^k$, $\mathbf{I}$ is an identity

matrix and the normalizing factor f_0^k is equal to

$$f_0^k = \frac{tr(\mathbf{G}_p^{k^T}\mathbf{G}_p^k)}{M}\,, \tag{25}$$

where tr is denotaded as the trace of the matrix $\mathbf{G}_p^{k^T}\mathbf{G}_p^k$ and M is the total number of dipoles composing the layer. From the correction $\boldsymbol{\Delta}\mathbf{p}^k = \mathbf{p}^{k+1} - \mathbf{p}^k$, we can conclude that the linear system to be solved is given by

$$\left[\mathbf{G}_p^{k^T}\mathbf{G}_p^k + \mu f_0^k \mathbf{I}\right]\mathbf{p}^{k+1} = \mathbf{G}_p^{k^T}\boldsymbol{\Delta}\mathbf{T}^o. \tag{26}$$

Owing to nonlinear relation of the magnetization direction $\mathbf{q}^k$ with the predicted total-field anomaly, the gradient vector and the Hessian matrix for this case are, respectively,

$$\mathbf{J}_q^k = -2\mathbf{G}_q^{k^T}[\boldsymbol{\Delta}\mathbf{T}^o - \boldsymbol{\Delta}\mathbf{T}(\mathbf{s}^k)] \tag{27}$$

and

$$\mathbf{H}_{qq}^k = 2\mathbf{G}_q^{k^T}\mathbf{G}_q^k \tag{28}$$

in which $\mathbf{G}_q^k$ is a $N \times 2$ sensitivity matrix, whose elements are composed by derivative of equation 19 in relation of each component of the vector $\mathbf{q}^k$, that are the inclination and declination, respectively. Nevertheless, in order to calculate the correction $\boldsymbol{\Delta}\mathbf{q}^k$ at the kth iteration, we use the Levernberg-Marquardt method (Aster et al., 2005) by solving the linear system

$$\left[\mathbf{G}_q^{k^T}\mathbf{G}_q^k + \lambda^k \mathbf{I}\right]\boldsymbol{\Delta}\mathbf{q}^k = \mathbf{G}_q^{k^T}[\boldsymbol{\Delta}\mathbf{T}^o - \boldsymbol{\Delta}\mathbf{T}(\mathbf{s}^k)], \tag{29}$$

where λ is the Marquardt parameter that is updated along the iterative process and $\mathbf{I}$ is an indentity matrix.

Iterative process for magnetization estimation

The estimation of the magnetic moments $\mathbf{p}^\sharp$ and the magnetization direction $\mathbf{q}^\sharp$ is formulated as an inverse problem of minimizing the difference between the observed data $\mathbf{\Delta T}^o$ and the predicted data $\mathbf{\Delta T}(\mathbf{s})$. As we can notice, the solution of the inversion is given by solving two linear systems, one shown in equation 26 and other in equation 29. For this reason, we propose a nested algorithm for solving the inverse problem in two steps.

Our iterative algorithm starts with an initial guess for the magnetization direction $\mathbf{q}_0$. At the kth iteration, we calculated a set of magnetic moment $\mathbf{p}^k$ by imposing a positivity constraint on equation 26. After estimating the magnetic-moment distribution $\mathbf{p}^k$ at the kth iteration using the previous estimate $\mathbf{q}^k$ for the magnetization direction, we estimate a new vector $\mathbf{q}^{k+1}$ by solving an unconstrained nonlinear inverse problem an applying the correction $\mathbf{\Delta q}^k$ using the equation 29. The iterative process stops when the minimum of the goal function (equation 19a) is reached. An overview of the algorith is shown in figure 2 and in the algorithm 1.

Algorithm 1: Nested NNLS and Levenberg-Marquardt method

Input : $\mathbf{\Delta T}^o$, $\mathbf{q}_0$

Output: $\mathbf{p}^\sharp$,$\mathbf{q}^\sharp$

while *(not converge) or* $(i < i_{max})$ **do**

  step 1: Solve equation 26 using NNLS ;

  step 2: Compute goal function (19) ;

  while *(not converge) or* $(j < j_{max})$ **do**

    step 3: Initialize the Levenberg-Marquardt algorithm ;

    step 4: Compute goal function (19);

    while $k < k_{marq}$ **do**

      step 5: Solve equation 29 ;

      step 6: Apply the correction for magnetization direction ;

      step 7: Compute goal function (19);

    end

    step 8: Analysis of convergence for inner loop.

  end

  step 9: Analysis of convergence for outer loop.

end

The choice of layer depth $\mathbf{z_c}$ and regularization parameter μ

The procedure for the use of our methodology for estimating the total magnetization require the choice of two main parameters. The first one is the layer depth z_c as shown in figure 1 and the second is the regularization parameter μ shown in equation 26.

The method of the choice of layer is based on a classical approach proposed by Dampney

(1969). The author pointed out that the layer depth should satisfy an interval from 2.5 to 6 times the grid spacing. It should be notice that this rule was applied on an evenly spaced data. However, the choice for applying our method should correspond to an interval from 2 to 3 times the greater grid spacing. It is necessarily to point out that this range of values was found empirically due to the application on a irregular grid data.

To solve the equation 26 we have to choose a reliable regularization parameter μ. For this purpose, we use the L-curve method (Hansen and OLeary, 1993). This approach is widely used in the literature to find a regularizing parameter, which filtering out enough noise whithout loosing to much information in the final solution. The procedure of finding the parameter is basically to plot a curve of optimal values between the solution norm and residual norm. The corner of the curve is the final result which gives a threshold between the regularization function and the data misfit.

APPLICATION TO SYNTHETIC DATA

We test the proposed method by applying it to three different synthetic data sets simulating complex geological scenarios. The first one is generated by a model containing a set of sources with different geometries, all of them with the same magnetization direction. The second data set is generated by a set of magnetized bodies, but one them is a shallow interfering source with the same magnetization direction. In the third test, we violate the unidirectional approach by simulating an interfering shallow source with different magnetization direction from the others bodies.

For all tests, the simulated data were computed on an irregular grid of 49×25 points (a total of $N = 1225$ observations) at a constant height of $100\,m$. We assume an observation area of extending $12\,km$ along the x- and y-axis, resulting a grid spacing of $250\,m$ and $500\,m$ on x- and y-axis, respectively. The data were contamined with pseudorandom Gaussian noise with zero mean and $10\,nT$ standard deviation. The main field direction simulated was $I = -40^\circ$ and $D = -22^\circ$ for the inclination and declination, respectively. For the inversion, we use an equivalent layer composed by a grid of 49×25 dipoles (a total of $M = 1225$ equivalent sources) positioned at a depth of $z_c = 1150\,m$ below the observation plane (2.5 times the greater grid spacing). We use the L-curve to choose the regularizing parameter (μ). The algorithm 1 starts with an initial guess $\mathbf{q}_0 = (-10^\circ, -10^\circ)$ for inclination and declination, respectively.

Unidirectional magnetization direction sources

In order to test the methodology, we generate a 3D prism with polygonal cross-section whose the top is positioned at a depth of $450\,m$ and the bottom $3150\,m$ with magnetization

intensity of $4\,A/m$. We also generate two spheres with radius equal to $500\,m$, one of them with the coordinates of center $x_c = 1800\,m$, $y_c = -1800\,m$ and $z_c = 1000\,m$ and the other with $x_c = 800\,m$, $y_c = 800\,m$ and $z_c = 1000\,m$. The magnetization intensity for the two both spheres is equal to $3\,A/m$. We produce two rectangular prisms with the same $2.5\,A/m$ of magnetization intensity. The smaller prism has the top at a depth of $450\,m$ and side lengths of $1000\,m$, $700\,m$ and $500\,m$ along x-,y- and z-axis, respectively. The greater prism has the top at a depth of $500\,m$ and side lengths of $1000\,m$, $2000\,m$ and $1550\,m$ along x-,y- and z-axis. All simulated sources have inclination $-25°$ and declination $30°$. The noise-corrupted data is shown in figure 3a.

Figure 3b shows the predicted data produced by equivalent layer. Figure 3c shows the residuals defined as the difference between the simulated data (figure 3a) and the predicted data (figure 3b). The residuals appear normally distributed with a mean of $-0.30\,nT$ and a standard deviation of $9.67\,nT$ as shown in figure 3d. The estimated magnetization direction $\mathbf{q}^\sharp$ has inclination $-28.6°$ and declination $30.8°$. Figure 3e shows the estimated magnetic-moment distribution $\mathbf{p}^\sharp$. The convergence of the algorithm 1 is shown in figure 3f. These results show that the all-positive magnetic-moment distribution and the estimated magnetization direction produce an acceptable data fitting.

Unidirectional model with shallow interfering source

In this section we test the methodology perfomance when exist a shallow interfering source. The model is almost the same as the previous section except the smaller prism. For this purpose, we put the top of the smaller prism at a depth of $150\,m$ and side lengths of $1000\,m$, $700\,m$ and $500\,m$ along x-,y- and z-axis, respectively. The magnetization intensity for this

prism is equal to $1.5\,A/m$. The magnetization direction of all sources is $-25°$ inclination and declination 30°, respectively. The synthetic data is shown in figure 4a.

Figure 4b shows the predicted total-field anomaly produced by equivalent layer. Figure 4c shows the residuals defined as the difference between the simulated data (figure 4a) and the predicted data (figure 4b). The residuals appear normally distributed with a mean of $-0.42\,nT$ and a standard deviation of $10.67\,nT$ as shown in figure 4d. The estimated magnetization direction $\mathbf{q}^\sharp$ has inclination $-28.7°$ and declination 31.7°. Figure 4e shows the estimated magnetic-moment distribution $\mathbf{p}^\sharp$. The convergence of the algorithm 1 is shown in figure 4f. Despite the residual located above the shallow magnetic source, we consider the methodology produced a reliable result. Therefore, that the all-positive magnetic-moment distribution and the estimated magnetization direction produce an acceptable data fitting.

Shallow source with different magnetization direction

In this test we simulate the presence of a shallow interfering body with different-magnetization direction from the other magnetic sources. The shallow prism has the dimension, the intensity magnetization and magnetization direction are equal to the previous section. However, the magnetization direction of the shallow prism is 20° inclination and declination $-30°$. The noise-corrupted data is shown in figure 5a.

Figure 5b shows the predicted total-field anomaly. Figure 5c shows the residuals defined as the difference between the simulated data (figure 5a) and the predicted data (figure 5b). The residuals have a mean of $-0.71\,nT$ and a standard deviation of $10.67\,nT$ as shown in figure 5d. The estimated magnetization direction $\mathbf{q}^\sharp$ has inclination $-30.4°$ and declination 27.6°. Figure 5e shows the estimated magnetic-moment distribution $\mathbf{p}^\sharp$. The convergence

of the algorithm 1 is shown in figure 5f. Despite the slight difference for the magnetization direction, the estimated magnetic-moment distribution produces an acceptable data fit. Another feature we can highlight is the data misfit just above the shallow prism with different magnetization direction.

APPLICATION TO FIELD DATA

The Goias alkaline province (GAP) is a region in the central part of Brazil that there are occurences of mafic-ultramafic alkaline magmatism. This region presents a variety of rocks with an extense petrographic types. Throughout the area there are mafic-ultramagic complexes (plutonic intrusions), subvolcaninc alkaline intrusions (diatremes) and volcanic products (kamafugite lava flows) with several dikes. Among the main alkaline complexes of GAP are the Montes Claros de Goias, Diorama, Corrego dos Bois, Morro do Macaco and Fazenda Buriti. These alkaline intrusions are sorrounded by a Precambrian basement and the Phanerozoic sedimentary rocks of the Paran basin. (Junqueira-Brod et al., 2005; Carlson et al., 2007; Marangoni and Mantovani, 2013; Dutra et al., 2014). Recent studies indicate the existence of a remarkable remanent magnetization component within these intrusions (Marangoni and Mantovani, 2013; Oliveira Jr et al., 2015; Marangoni et al., 2016; Zhang et al., 2018).

This area was the target of an aeromagnetic survey with a financial support from the government of the state of Goias (LASA Prospection and Engineer, 2004). This survey has a flight pattern with North-South spaced from $\sim 500\,m$ and $\sim 8\,m$ along each line, and a constant height of $100\,m$ from the terrain. The main field direction for this area was $-19.5°$ and $-18.5°$ for inclination and declination, respectively. In order to test the methodology on a field data, we invert the data from the alkaline complex of Montes Claros. To speed up data processing and inversion, we downsampled the data along the flight lines, resulting a grid of 55×32 points (a total of $N = 1787$ observations). This new set up results an approximately $320\,m$ and $470\,m$ grid spacing along the x- and y-axis, respectively. Figure 6a shows the observed data from the complex of Montes Claros. For the inversion, we use

an equivalent layer composed by a grid of 55×32 dipoles (a total of $M = 1787$ equivalent sources) positioned at a depth of $840\,m$ below the observation plane (~ 2 times the greater grid spacing). The algorithm 1 starts with an initial guess of $-70°$ and $50°$ for the inclination and declination, respectively. Figure 6b shows the predicted data produced by equivalent layer. Figure 6c shows the residuals defined as the difference between the observed data (figure 6a) and the predicted data (figure 6b). The histogram of residuals (figure 6d) presents a mean of $-14.52\,nT$ ($\sim 0.1\%$ of the maximum value of total-field anomaly data) and standard deviation of $312.28\,nT$ ($\sim 2\%$ of the maximum value of total-field anomaly data). The estimated magnetization direction $\mathbf{q}^\sharp$ has inclination $-50.2°$ and declination $34.9°$. Figure 6e shows the estimated magnetic-moment distribution $\mathbf{p}^\sharp$. The convergence of the algorithm 1 is shown in figure 6f. We check the quality of the estimated magnetization direction by computing the reduction-to-pole of the observed total-field anomaly. Figure 7 shows the RTP anomaly. As we can notice from this last figure is that the RTP field exhibits predominantly positive values and decays to zero towards the borders of study area. For this reason, we consider that the estimated magnetization direction led to a satisfactory RTP anomaly. We conclude with these results that the all-positive magnetic moment distribution and the estimated magnetization direction produce an acceptable data fitting. The estimated magnetization direction also confirms the existence of remarkable remanent magnetization for these instrusions.

REFERENCES

Aster, R. C., B. Borchers, and C. H. Thurber, 2005, Parameter estimation and inverse problems (international geophysics): Academic Press.

Baratchart, L., D. P. Hardin, E. A. Lima, E. B. Saff, and B. P. Weiss, 2013, Characterizing kernels of operators related to thin-plate magnetizations via generalizations of Hodge decompositions: Inverse Problems, **29**, 015004(29pp).

Blakely, R. J., 1996, Potential theory in gravity and magnetic applications: Cambridge University press.

Carlson, R. W., A. L. N. Araujo, T. C. Junqueira-Brod, J. C. Gaspar, J. A. Brod, I. A. Petrinovic, M. H. B. M. Hollanda, M. M. Pimentel, and S. Sichel, 2007, Chemical and isotopic relationships between peridotite xenoliths and maficultrapotassic rocks from southern brazil: Chemical Geology, **242**, 415 – 434.

Dampney, C. N. G., 1969, The equivalent source technique: GEOPHYSICS, **34**, 39–53.

Dutra, A. C., Y. Marangoni, and R. I. F. Trindade, 2014, Aeromagnetic and physical-chemical properties of some complexes from GoiÃ¡s Alkaline Province: Brazilian Journal of Geology, **44**, 361 – 373.

H. Goldstein, C. P. P. J., and J. L. Safko, 1980, Classical mechanics: Addison-Wesley.

Hansen, P., and D. OLeary, 1993, The use of the l-curve in the regularization of discrete ill-posed problems: SIAM Journal on Scientific Computing, **14**, 1487–1503.

Junqueira-Brod, T. C., J. C. Gaspar, J. A. Brod, and C. V. Kafino, 2005, Kamafugitic diatremes: their textures and field relationships with examples from the gois alkaline province, brazil: Journal of South American Earth Sciences, **18**, 337 – 353. (Volcanic rocks in Brazil through time and different tectonic settings).

Lawson, C. L., and R. J. Hanson, 1974, Solving least squares problems: SIAM.

Li, Y., M. Nabighian, and D. W. Oldenburg, 2014, Using an equivalent source with positivity for low-latitude reduction to the pole without striation: GEOPHYSICS, **79**, J81–J90.

Lima, E. A., and B. P. Weiss, 2016, Ultra-high sensitivity moment magnetometry of geological samples using magnetic microscopy: Geochemistry, Geophysics, Geosystems, **17**, 3754–3774.

Marangoni, Y., H. Zhang, and H. Ferreira, 2016, Gravity and magnetic integrated data interpretation of the corrgo dos bois complex, gois alkaline province, central brazil: Revista Brasileira de Geofsica, **33**, 599–610.

Marangoni, Y. R., and M. S. Mantovani, 2013, Geophysical signatures of the alkaline intrusions bordering the paran basin: Journal of South American Earth Sciences, **41**, 83 – 98. (Alkaline Magmatism and the Lithospheric Mantle : a special issue in honour of the work of Celso de Barros Gomes on the occasion of his 77th birthday).

Oliveira Jr, V. C., D. P. Sales, V. C. F. Barbosa, and L. Uieda, 2015, Estimation of the total magnetization direction of approximately spherical bodies: Nonlinear Processes in Geophysics, **22**, 215–232.

Pedersen, L. B., 1991, Relations between potential fields and some equivalent sources: GEOPHYSICS, **56**, 961–971.

Zhang, H., D. Ravat, Y. R. Marangoni, G. Chen, and X. Hu, 2018, Improved total magnetization direction determination by correlation of the normalized source strength derivative and the rtp fields: GEOPHYSICS, **0**, 1–45.

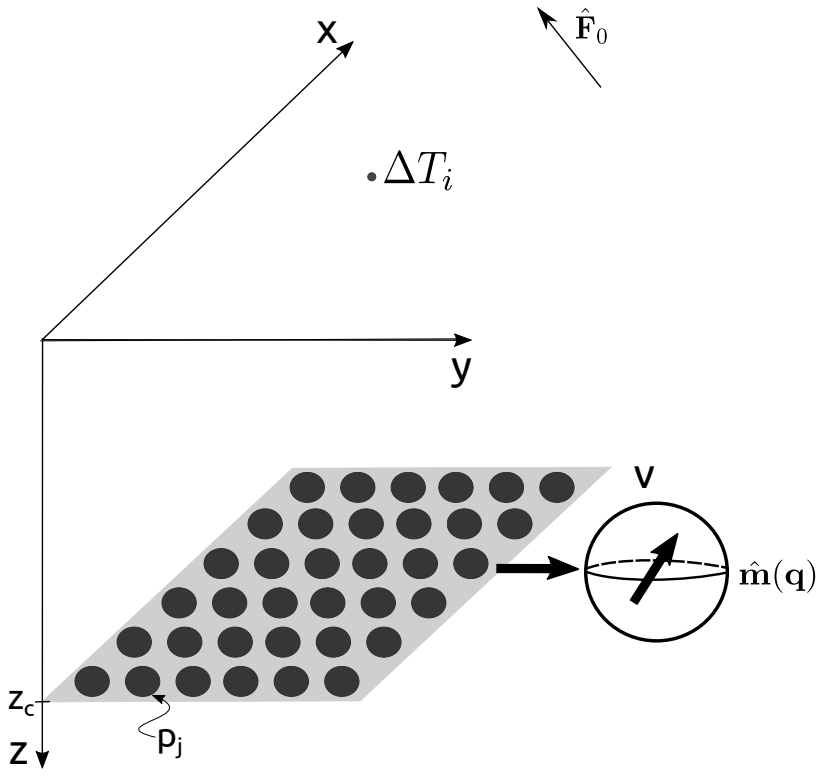

Figure 1: Schematic representation of an equivalent layer. The layer is positioned over the horizontal plane at a depth of $z = z_c$. $\Delta T_i = f_i(\mathbf{s})$ is the predicted total-field anomaly at the point (x_i, y_i, z_i) produced by the set of M equivalent sources (black dots). Each source is located at the point (x_j, y_j, z_c), $j = 1, \ldots, M$, and represented by a dipole with unity volume υ with magnetization direction $\hat{\mathbf{m}}(\mathbf{q})$ and magnetic moment p_j.

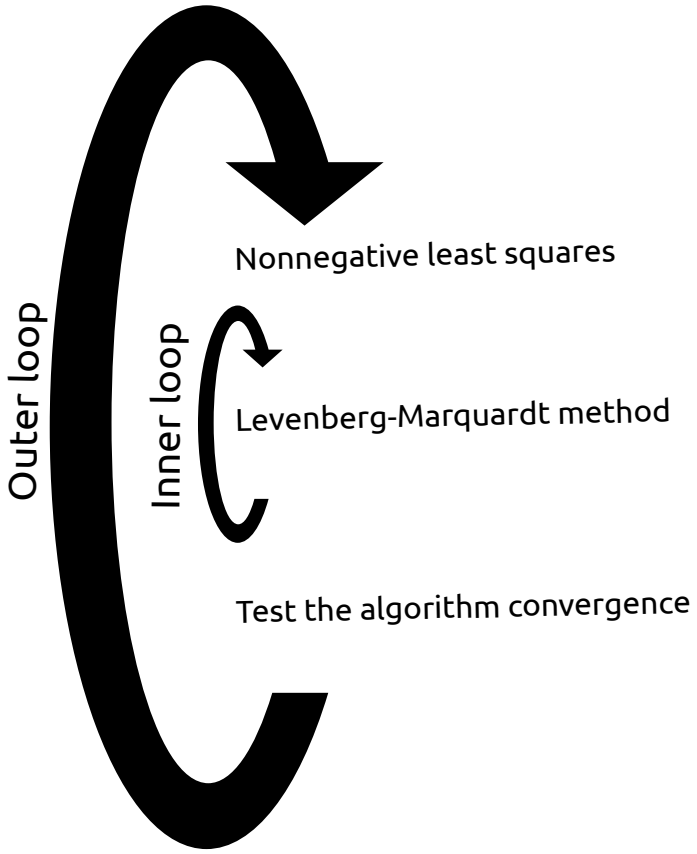

Figure 2: Iterative scheme overview for NNLS and Levenberg-Marquardt method for estimating magnetization direction. The outer loop is the nonnegative solution for magnetic-moment distribution and the inner loop calculates the magnetization direction correction using Levenberg-Marquardt method.

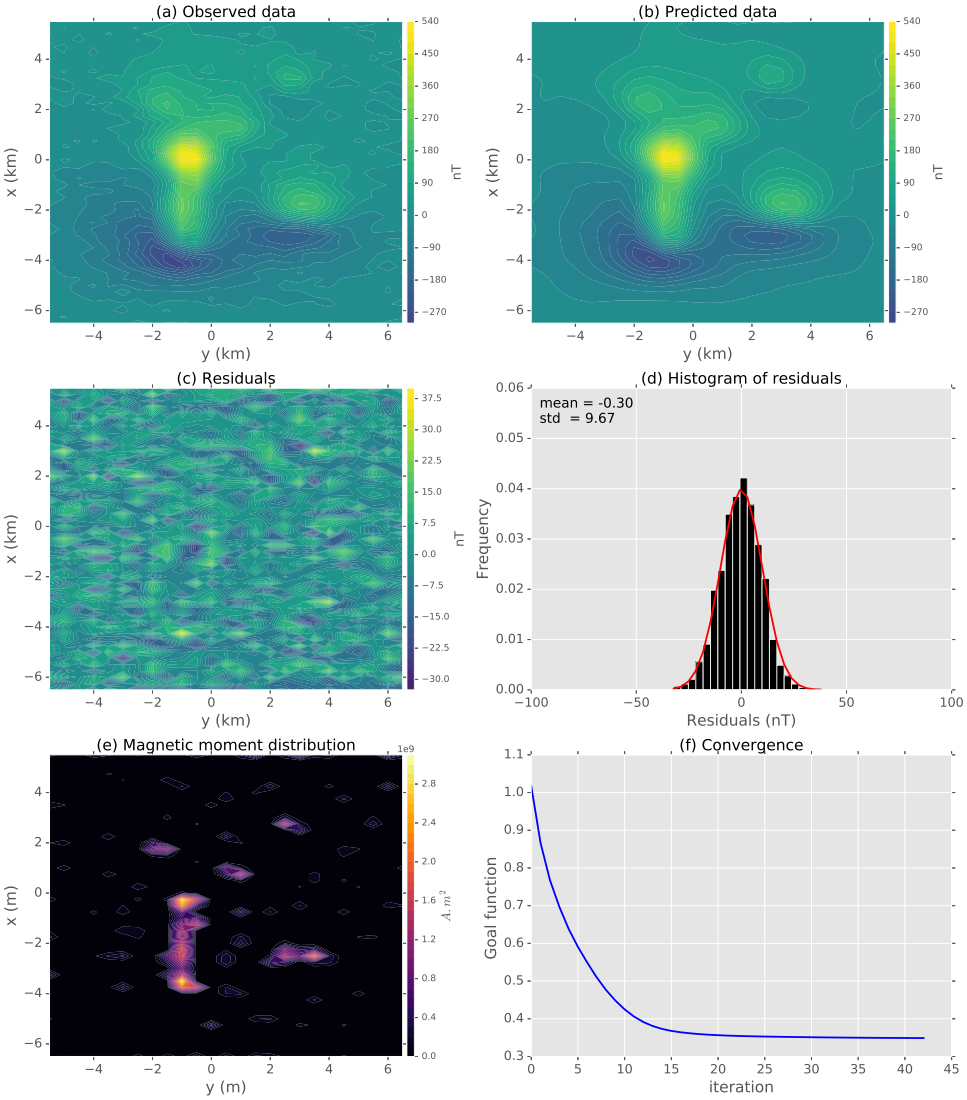

Figure 3: Application to synthetic data for unidirectional model. (a) Noise-corrupted data. (b) Predicted data produced by equivalent layer. (c) Difference between the data shown in panels (a) and (b). (d) Histogram of residuals. (e) All-positive magnetic moment distribution. (f) Goal function value (equation 19a) per iteration showing the convergence.

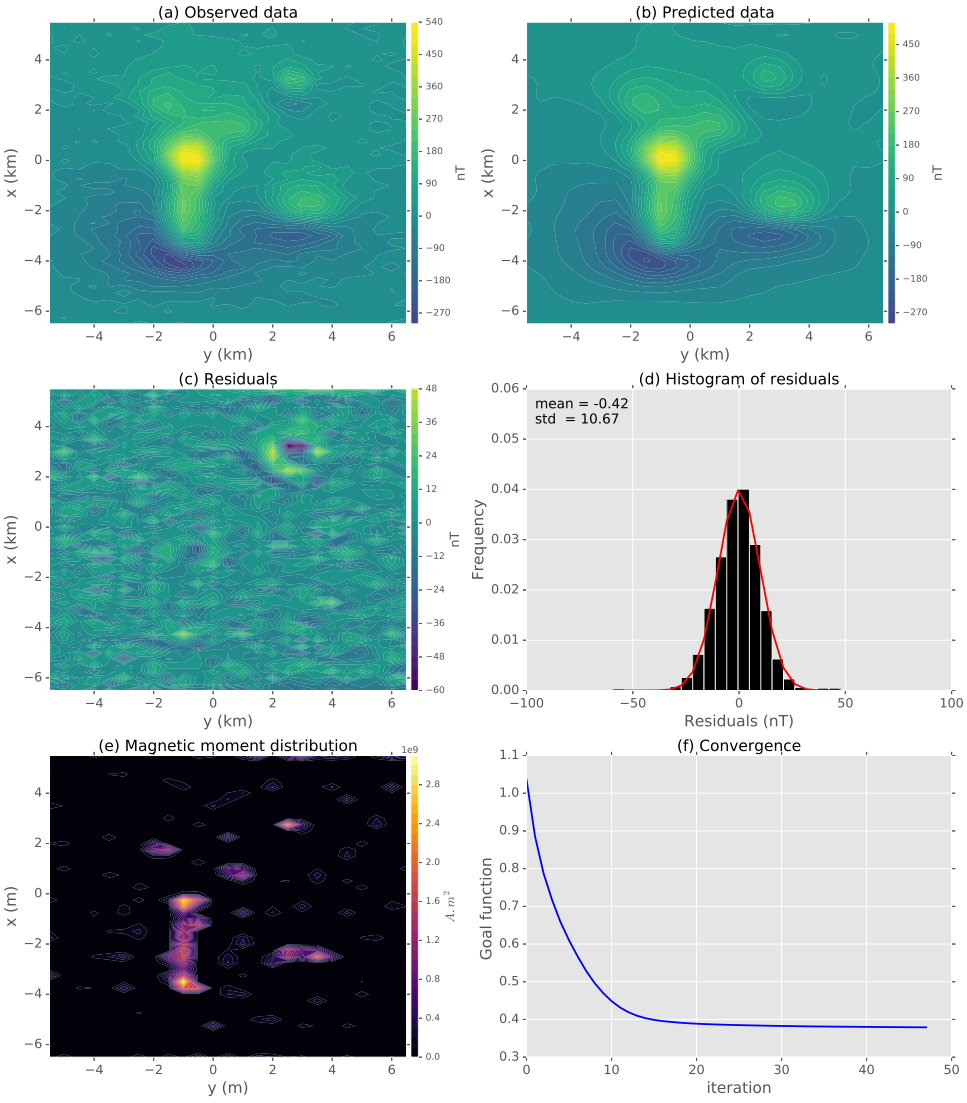

Figure 4: Application to synthetic data with a shallow interfering source. (a) Noise-corrupted data. (b) Predicted data produced by equivalent layer. (c) Difference between the data shown in panels (a) and (b). (d) Histogram of residuals. (e) All-positive magnetic moment distribution. (f) Goal function value (equation 19a) per iteration showing the convergence.

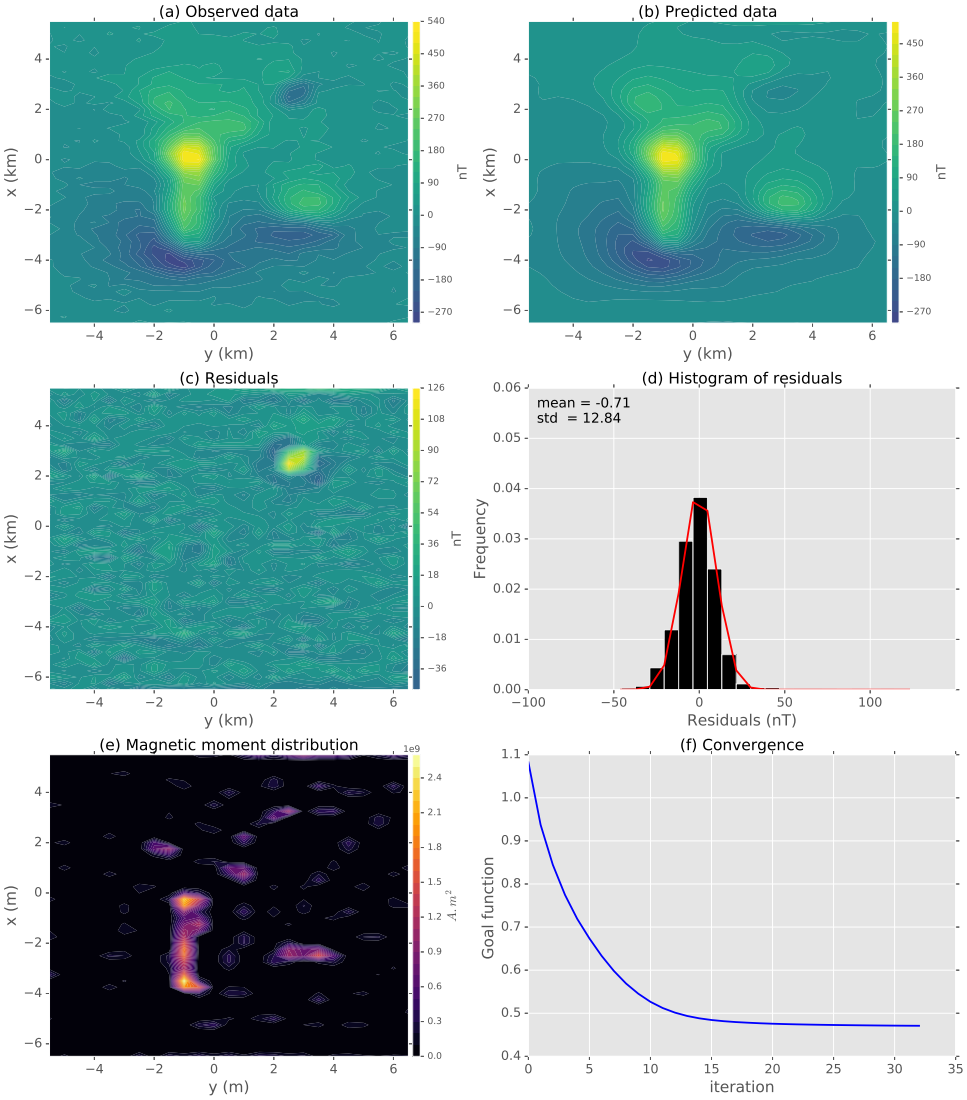

Figure 5: Application to synthetic data with a shallow interfering source with different magnetization direction. (a) Noise-corrupted data. (b) Predicted data produced by equivalent layer. (c) Difference between the data shown in panels (a) and (b). (d) Histogram of residuals. (e) All-positive magnetic moment distribution. (f) Goal function value (equation 19a) per iteration showing the convergence.

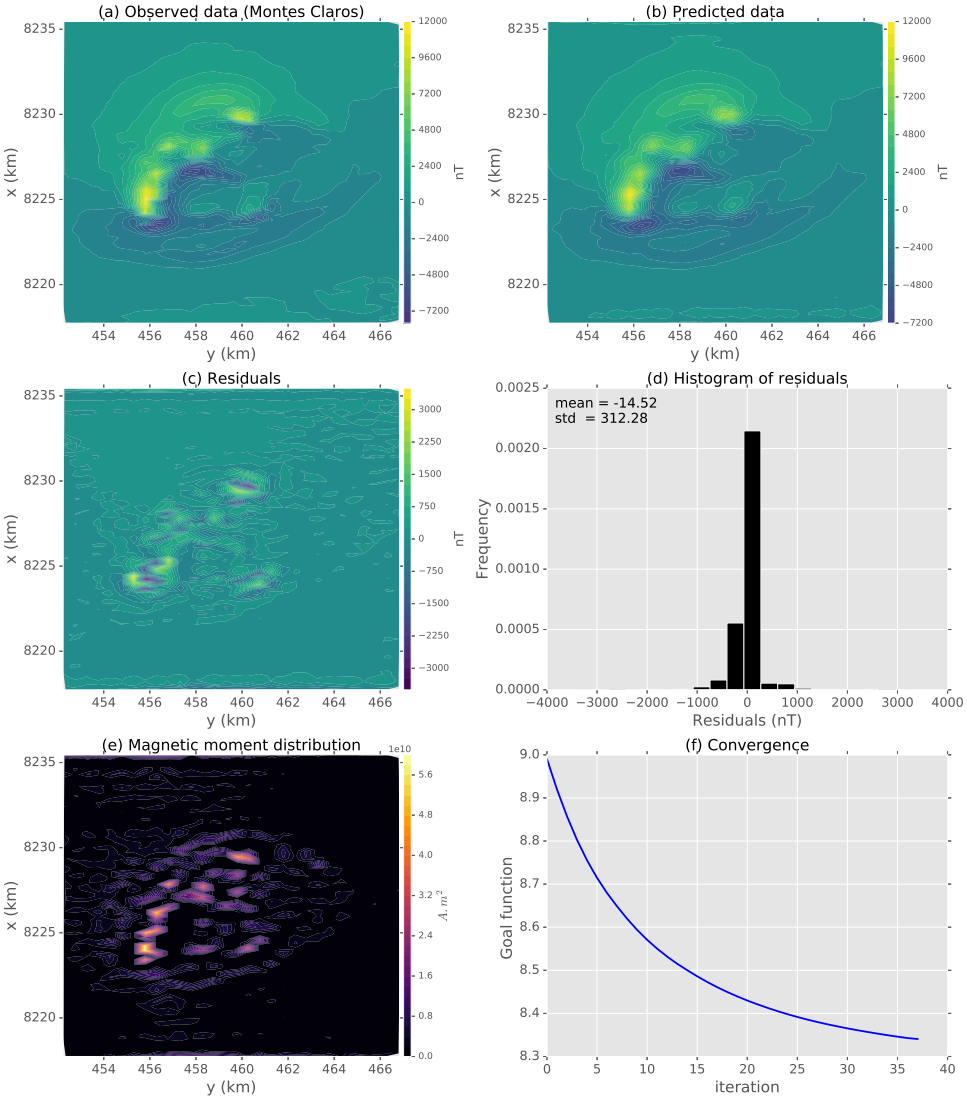

Figure 6: Application to field data located in complex of Montes Claros. (a) Observation data. (b) Predicted data produced by equivalent layer. (c) Difference between the data shown in panels (a) and (b). (d) Histogram of residuals. (e) All-positive magnetic moment distribution. (f) Goal function value (equation 19a) per iteration showing the convergence.

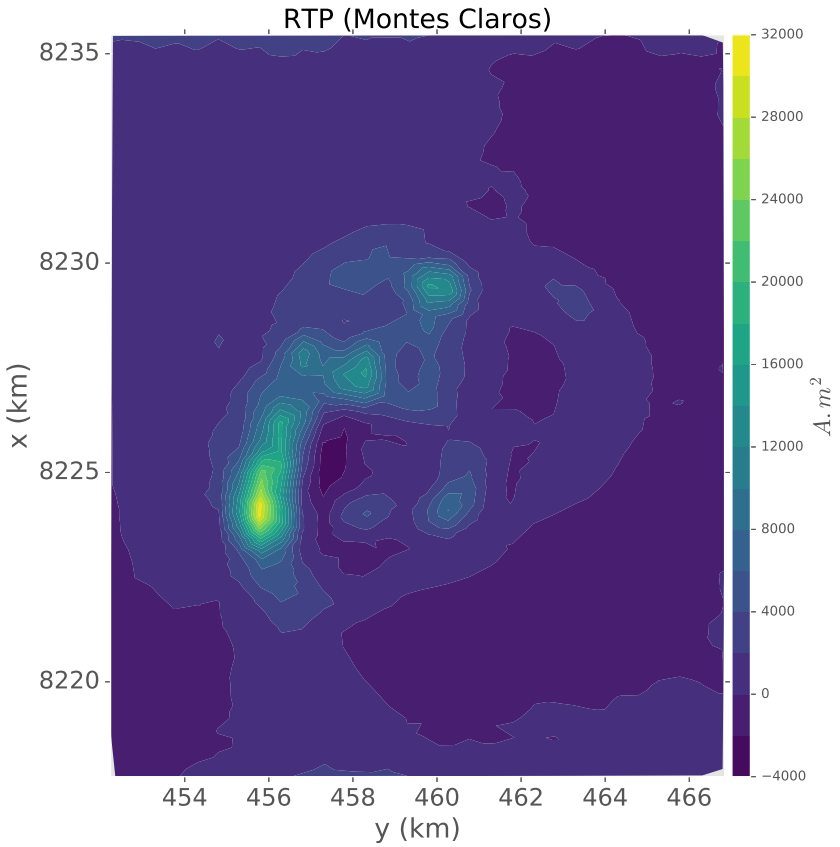

Figure 7: Application to field data located in complex of Montes Claros. RTP anomaly computed by using the estimated magnetization distribution shown in figure 6e.